

Reconstructed soil moisture droughts in Belgium reveal 2011–2020 was the driest decade since 1970

Katoria Lekarkar^{*1}, Rohini Kumar², Oldrich Rakovec³, Stefaan Dondeyne^{1,4,6},
and Ann van Griensven^{1,5}

¹Department of Water and Climate, Vrije Universiteit Brussel, Pleinlaan 2,
1050 Brussels, Belgium

²UFZ-Helmholtz Centre for Environmental Research, Permoserstraße 15,
04318 Leipzig, Germany

³Faculty of Environmental Sciences, Czech University of Life Sciences
Prague, Praha-Suchdol, Czech Republic

⁴Gembloux Agro-Bio Tech, University of Liège, Pass. des Déportés 2, 5030
Gembloux, Belgium

⁵Water Science & Engineering Department, IHE Delft Institute for Water
Education, 2611 AX Delft, The Netherlands

⁶Department of Soil Science and Land Resources, Universitas Padjadjaran,
Jawa Barat 45363, Bandung, Indonesia

Abstract

In recent years, Belgium has experienced a sequence of intense droughts with wide-ranging impacts across multiple sectors. Determining whether these events are unprecedented or within natural variability requires indicators that properly diagnose drought. Root-zone soil moisture is a suitable indicator because it integrates meteorological forcings with land-surface processes. In Belgium, however, operational monitoring relies mainly on precipitation-based indices and lacks long-term in situ soil-moisture observations, leaving uncertainty about whether these indices capture the persistence of root-zone drought. To address this gap, we reconstructed daily root-zone soil-moisture dynamics over Belgium for 1970–2020 using the mesoscale Hydrologic Model (mHM), placing recent droughts in

^{*}Corresponding author: katoria.lesaalon.lekarkar@vub.be

27 historical context and evaluating the adequacy of precipitation-based indicators for repre-
28 senting drought conditions. Our analysis shows that droughts in 2011–2020 were unprece-
29 dented in both duration and severity over the past five decades. Between 2011 and 2020,
30 the country experienced a cumulative three years (non-consecutive) of drought exposure,
31 representing 30% of the decade. This more than doubles the cumulative duration in each
32 decade from 1981–2010 and about 1.5 times that of 1971–1980.

33 We further find that the Standardized Precipitation–Evapotranspiration Index (SPEI),
34 currently used operationally as a proxy for agricultural droughts in Belgium, underes-
35 timates the persistence of root-zone droughts because it does not explicitly account for
36 land-surface memory. Thus, by including soil moisture monitoring in drought assessment,
37 residual stresses on agriculture and subsurface water which can persist long after meteo-
38 rological conditions have normalized, can still be detected. This gives decision-makers a
39 more realistic understanding of droughts and how to respond proportionately.

40 **Keywords:** Mesoscale, climate variability, drought persistence, cumulative exposure, agri-
41 cultural drought monitoring

42 1 Introduction

43 Belgium has faced a succession of hugely consequential droughts in recent years. These
44 droughts ~~led to declined suppressed~~ crop yields, increased water scarcity ~~and restricted~~
45 ~~water abstractions~~, disrupted navigation on inland waters and caused economic losses run-
46 ning into millions of Euros (Tröltzsch et al., 2016; De Ridder et al., 2020). ~~Between January~~
47 ~~and~~

48 ~~The country has faced at least five major droughts between 2011 and 2023. From~~
49 ~~January to April 2011, Belgium had only the country had~~ received less than ~~50% of the~~
50 ~~climatologically half of the~~ expected rainfall by that time of the year (European Commis-
51 sion, Joint Research Centre, 2011). ~~In 2018-2019, a~~ ~~This was followed by successive~~ multi-
52 ~~year drought characterized by rainfall deficits and record-breaking temperatures swept through~~
53 ~~the country, causing significant economic costs across different sectors~~ ~~droughts in 2016-2017~~
54 ~~and then 2018-2019, which compounded water scarcity with unprecedented temperatures,~~
55 ~~including a record temperature of 39.7°C in July 2019~~ (Bastos et al., 2020; Chini, 2022).
56 ~~The consequences to different sectors were enormous.~~ In the Flemish region (the north-
57 ern part of the country), the ~~event 2018-2019 drought~~ reduced potato production by 31%,
58 leading to a 23% surge in prices. Sugar beet production ~~also~~ fell by 13% ~~and cereal yields~~
59 ~~reduced by while cereal yields experienced a 10% decline.~~ These led to farmers submitting
60 claims of about 150 million to the Flemish Disaster Fund to compensate for losses from
61 the drought (De Ridder et al., 2020). According to ~~De Vlaamse Waterweg nv~~, the agency
62 in charge of inland water in Flanders (~~De Vlaamse Waterweg nv~~), inland navigation suf-
63 fered economic losses ~~of more than exceeding~~ 300 million due to low water levels ~~during~~
64 ~~the 2018-19 drought. In July 2019, a temperature record of 39.7°C was measured, which~~
65 ~~marked the most intense heatwave ever recorded in the country at the time. Soon after, in~~

66 navigable waterways.

67 The country experienced another drought crisis in 2022, ~~another drought hit Belgium,~~
68 ~~affecting 53.4~~ where more than 50% of the country was affected, more than ten times
69 the long-term average impacted area of 4.6% between 2000 and 2020. ~~According to the~~
70 ~~Copernicus Climate Change Service (), surface soil moisture in Europe throughout 2022~~
71 ~~was the second lowest in the last 50 years , sustained by higher-than-average temperatures~~
72 ~~and a sequence of heatwaves that started in spring and continued throughout summer~~The
73 conditions were so dry that the country experienced a record low 5 mm precipitation in July
74 that year, the lowest in 137 years (since 1885). The precipitation deficit drove groundwater
75 levels to their lowest since at least 2000 (DOV, 2025); in many locations, levels did not
76 fully recover over the following winter (VMM, 2023). Of all European countries, Bel-
77 gium was the second most affected country in terms of the proportion of area impacted
78 by the drought (European Environment Agency, 2023). ~~By March that year, water levels~~
79 ~~in half of the groundwater wells in Flanders were very low for that time of the year. By~~
80 ~~May, this number had increased to two-thirds . In July, rainfall in the country was the~~
81 ~~lowest in 137 years(since 1885), with an average rainfall of 5 mm across the country.~~
82 ~~The drought caused significant crop damage, and the Flemish government subsequently~~
83 ~~declared~~ According to the Copernicus Climate Change Service, 2022, surface soil moisture
84 in Europe throughout 2022 was the second lowest in the previous 50 years, sustained
85 by higher-than-average temperatures and a sequence of heatwaves that started in spring
86 and continued throughout summer. The severity of the 2022 season eventually forced the
87 Flemish government to officially declare the drought a disaster ~~, which paved the way for~~
88 ~~farmers to seek compensation for crop losses. Evidently, these recent drought events to~~
89 provide compensation for widespread crop failures.

90 While the impacts of these recent droughts are well documented. ~~In order to contextualize~~
91 ~~their magnitudes and severity,~~ their rarity in a multi-decadal context is less well understood.
92 To place their magnitude and severity in perspective, it is therefore essential to reconstruct
93 historical drought ~~occurrences~~ occurrence over a sufficiently long climatological period.
94 ~~Such a~~ This long-term ~~perspective is necessary to determine whether recent droughts are~~
95 view allows us to assess whether recent events represent unprecedented extremes or ~~if they~~
96 fall within the range of natural climate variability.

97 Belgium has an extensive network of precipitation, river discharge and groundwater
98 monitoring stations which ~~provided~~ provide the basis for monitoring hydrological and me-
99 teorological droughts. This data underlies the drought indices found in dedicated platforms
100 for tracking and communicating the evolution of droughts across the country (e.g. <https://www.meteo.be/en/weather/forecasts/drought>, <https://vmm.vlaanderen.be/water/droogte>). ~~However, due~~ Due to the lack of long-term observations of soil moisture
101 in the country, the extent of agricultural droughts is presently evaluated with the Standard-
102 ized Precipitation Evaporation Index (SPEI) (Vicente-Serrano et al., 2010) which expresses
103 anomalies in the climatic water balance, that is, precipitation minus potential evapotran-
104 spiration. The nationwide drought conditions are reported through <https://www.meteo.be>.

107 be/en/weather/forecasts/drought. Although useful, ~~precipitation~~-~~precipitation~~- and
108 temperature-based drought indices are constrained by their limited ability to fully represent
109 agricultural drought conditions. Firstly, these indices do not explicitly account for the verti-
110 cal distribution of water within the root zone that supports plant growth, nor do they reflect
111 the complex interactions between soil moisture and vegetation across different stages of
112 plant development and are thus inadequate to represent extreme water shortage that would
113 lead to biomass and crop yield reduction (Sheffield et al., 2004; Mishra and Singh, 2010;
114 Samaniego et al., 2013). While soil moisture may exhibit a direct link to precipitation at
115 monthly timescales, soil moisture responses can be nonlinear at shorter timescales, partic-
116 ularly during dry conditions. Soil moisture also has a memory effect that can lag precip-
117 itation anomalies by days to months and in turn prolong the persistence and severity of
118 drought (Bonan and Stillwell-Soller, 1998; Nicholson, 2000; Wu et al., 2002; Seneviratne
119 et al., 2006). Accordingly, developing indices based on soil moisture offers a more reliable
120 indicator of agricultural drought, as soil moisture integrates the effects of antecedent pre-
121 cipitation, plant water uptake through transpiration, and the increasing persistence of soil
122 wetness with soil depth (Wu et al., 2002; Sheffield et al., 2004).

123 The goal of this study is therefore to perform a retrospective high-resolution recon-
124 struction of ~~root-zone~~-~~root-zone~~ soil moisture to perform a first-of-its-kind assessment of
125 soil moisture droughts in Belgium over the five decades between 1970 and 2020. We aim
126 to characterize major droughts that have occurred over this period by clustering soil mois-
127 ture anomalies using thresholds that capture the spatiotemporal characteristics of identified
128 events and rank them based on their magnitude, spatial extent and duration, and evaluate
129 how drought patterns in the country have evolved over the five decades. ~~In our study we~~
130 ~~use the mesoscale hydrological model (mHM) driven by offline meteorological forcings~~
131 ~~to simulate soil moisture conditions and derive grid-cell-level statistical distributions for~~
132 ~~characterizing the spatial and temporal patterns of agricultural drought over Belgium.~~ To
133 evaluate the correspondence between SPEI and soil moisture-based anomalies to represent
134 agricultural droughts, we compare SPEI at different accumulation periods to a soil mois-
135 ture index (SMI) (Samaniego et al., 2018) ~~, derived from monthly percentile ranking of soil~~
136 ~~moisture fields,~~ during selected major drought events.

137 2 Methodology

138 2.1 Study domain

139 Belgium is located in Western Europe covering an area of 30,528 km², varying in topog-
140 raphy from sea level along the North Sea coast to 700 m in the Ardennes-Eifel massif in
141 the south eastern parts (Figure 1) (Meersmans et al., 2016; Sousa-Silva et al., 2016). The
142 country experiences a warm temperate maritime climate (Köppen-Geiger Cfb) strongly
143 modulated by the warming effect of the North Atlantic Drift (Epicum et al., 2018; Beck
144 et al., 2023). Data from the Royal Meteorological Institute of Belgium (RMI) shows that

145 mean annual temperature ranges between 13 and 17 °C, varying spatially with elevation and
 146 distance inland. Winters are generally mild, with December–January lows dipping under
 147 5°C but rarely below freezing conditions for /periods. Winters are colder in the Ardennes
 148 region due to a weaker maritime influence and higher elevation. Summers are moderately
 149 warm with July highs peaking around 18°C although extremes above 30°C have occurred in
 150 recent years. The country receives an annual average precipitation of about 800 mm which
 151 varies between 700 mm in the western low lying regions, up to 1400 mm in the Ardennes
 152 where precipitation is enhanced by orographic effects (Erpicum et al., 2018). Temporally,
 153 rainfall is fairly evenly distributed throughout the year (Figure 1), with seasonal patterns
 154 dominated by summer convective storms and winter frontal systems (Brisson et al., 2011;
 155 Goudenhoofdt and Delobbe, 2013; Journée et al., 2015).

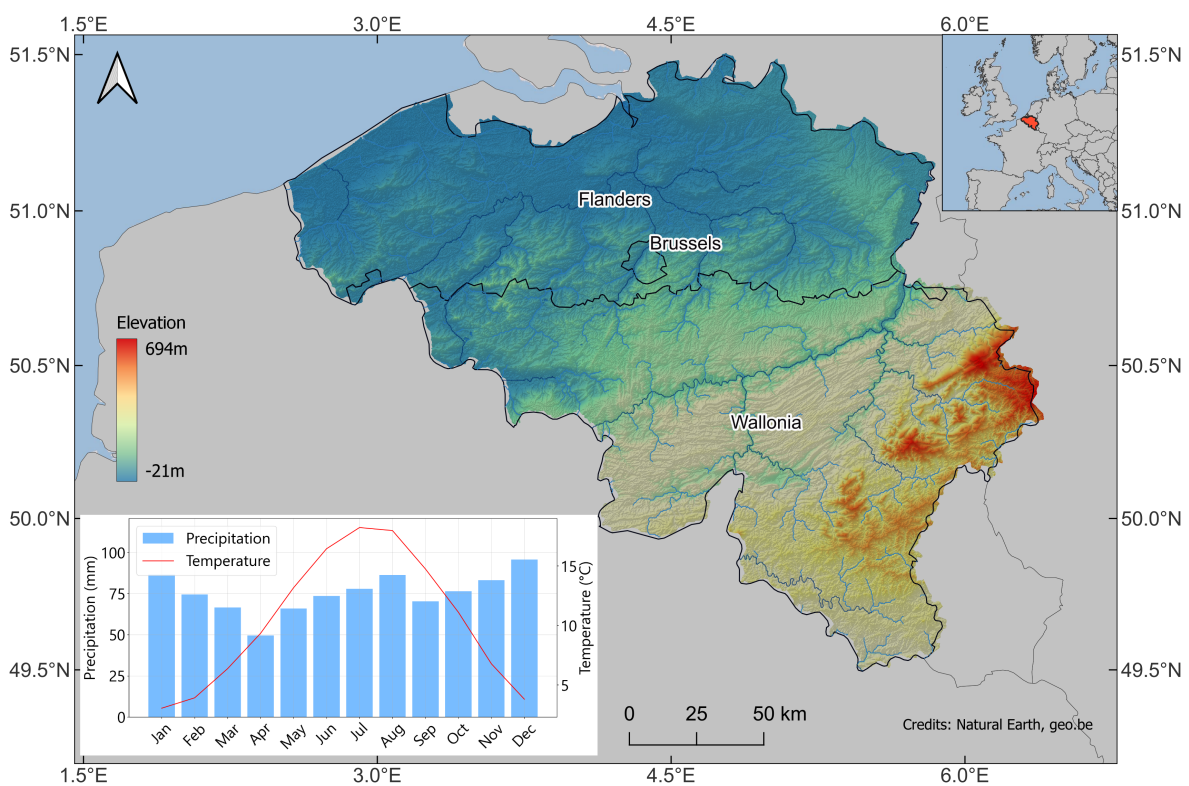


Figure 1: Topographic map of Belgium. The Ardennes region is distinguishable by its high elevation in the south east. Monthly mean precipitation and temperature in the inset plot are derived from data provided by The Royal Meteorological Institute of Belgium for the climatological period 1994-2023.

156 Land cover in the country is predominantly agricultural (44%), dominated by croplands
 157 and animal husbandry. Cultivated areas dominate the central loamy belt and the north-
 158 west of the country while the coastal polders typified by heavy soils, are more suited for
 159 animal-based farming (Beckers et al., 2018; Beckers et al., 2020; Statbel, 2025a). Forests
 160 cover about 23% of the territory (just over 700,000 hectares) with 79.8% in the Walloon
 161 region, 19.9% in Flanders and 0.3% in the Brussels-Capital (Sousa-Silva et al., 2016; Royal

162 Forestry Society of Belgium, 2025). Most of the lowland forests are dominated by broad-
163 leaved tree species with clusters of coniferous forest plantations in the north east. In the
164 Ardennes, forests form a mixed broadleaved–coniferous complex in the foothills, gradu-
165 ally transitioning to conifer-dominated stands at higher elevations (Royal Forestry Society
166 of Belgium, 2025; Statbel, 2025a). Built-up and urbanized areas account for about 20% of
167 the land with most cities dating back to the Middle Ages. The average population density
168 of the country is 385 inhabitants/km² (Beckers et al., 2020; Statbel, 2025b).

169 2.2 The mesoscale Hydrologic Model

170 ~~We~~ In our study, we used the mesoscale Hydrologic Model (mHM; Samaniego et al., 2010;
171 Kumar et al., 2013) (version v-5.13.2-dev0) to simulate domain-wide ~~root-zone~~ root-zone
172 (0-2 m) soil moisture conditions and streamflow, which we used as an additional hydrologic
173 constraint for validating basin-scale hydrology at major outlets.

174 mHM is a spatially distributed hydrological model based on numerical representations
175 of dominant hydrological processes. The model is driven by hourly to daily meteorolog-
176 ical forcings, which include precipitation, ~~temperature~~ air temperature (henceforth simply
177 temperature), and potential evapotranspiration, and accounts for major hydrological pro-
178 cesses like ~~snow-melt~~ snowmelt and accumulation, canopy storage, evapotranspiration,
179 surface runoff and flood routing, three-layer soil moisture content, and subsurface stor-
180 age. To represent spatial variability of inputs and state variables, the model uses three
181 different spatial resolutions, namely (in order of fine to coarse resolution) ~~÷~~ Level-0 (L_0 :
182 ~~small-scale~~ small-scale morphology) to represent the main terrain features, geological fea-
183 tures, land cover, and soil properties; Level-1 (L_1 : mesoscale hydrology) to represent the
184 dominant hydrological processes; and Level-2 (L_2 : ~~large-scale~~ large-scale meteorology) to
185 describe the variability of meteorological forcings. ~~mHM~~ The model harmonizes the data
186 internally using the multiscale parameter regionalization (MPR; Samaniego et al., 2010).
187 MPR links model parameters at L_1 to their corresponding ones at L_0 using ~~multiscale~~
188 ~~parameter regionalization~~. ~~This technique uses~~ non-linear transfer functions that couple
189 catchment characteristics with global (calibration) parameters to regionalize model hydro-
190 logic parameters at L_0 and link them to their corresponding values at L_1 using upscaling
191 operators such as arithmetic mean, geometric mean, and harmonic mean (MPR; Livneh
192 et al., 2015). With this technique, mHM ~~overcomes the problem of overparameterization~~
193 ~~and model equifinality~~ achieves quasi scale-invariant parameters that enable the model to
194 preserve the spatial variability of state variables and conserve mass balance (Samaniego
195 et al., 2010; Samaniego et al., 2011; Kumar et al., 2013; Samaniego et al., 2013). mHM
196 has been successfully used in multiple studies at scales ranging from river basins (Zink
197 et al., 2017; Dembélé et al., 2020; Demirel et al., 2024; Banjara et al., 2025), country
198 level (Samaniego et al., 2013; Rakovec et al., 2019; Boeing et al., 2022) up to continental-
199 scale (Samaniego et al., 2018; Moravec et al., 2019; Kumar et al., 2025) and global studies
200 (Řehoř et al., 2025; Shrestha et al., 2025).

2.2.1 Input data

~~Without long-term in situ soil moisture within Belgium to validate the soil moisture output of mHM, we expanded the model domain to cover parts of France, Germany and The Netherlands where soil moisture observations are available from the International Soil Moisture Network (ISMN). From the ISMN, we used data from the following networks: COSMOS, GROW, TERENO, BFG-Nw and ORACLE, all shown in Figure 2. We subsequently forced the model with~~ Our simulation is driven by daily fields of precipitation and temperature from the ENSEMBLES gridded dataset (E-OBS) version 30.0e (Cornes et al., 2018), which covers the entire modelling domain. E-OBS is a daily land-only gridded observational dataset over Europe which blends station network time series from the European National Meteorological and Hydrological Services or other sources and is provided with spatial resolutions of 0.1^0 and 0.25^0 . Our setup uses the 0.1^0 resolution product (access url: <https://cds.climate.copernicus.eu/datasets/insitu-gridded-observations-europe?tab=download>, last accessed March 2025). Since E-OBS does not provide potential evapotranspiration data, we generated this from the E-OBS minimum and maximum temperature using the method of Hargreaves and Samani, 1985.

The morphological datasets for the model originate from different sources ~~namely;~~, namely, LAI maps from Global Inventory Modeling and Mapping Studies (GIMMS) (Cao et al., 2023), DEM from the Shuttle Radar Topography Mission (Farr et al., 2007), land use data from Corine ~~Landcover~~ Land Cover (<https://land.copernicus.eu/en/products/corine-land-cover>), soil texture and bulk density data from the Harmonized World Soil Database (Nachtergaele et al., 2023), and geology datasets from the Global Lithological Map Database (Hartmann and Moosdorf, 2012), accessed from the url: <https://www.geo.uni-hamburg.de/geologie/forschung/aquatische-geochemie/glim.html> (last accessed February 2025). To ensure the spatial consistency required by mHM, we prepared all L_0 datasets at 0.001953125° ($1/512^\circ$), bilinearly coarsened the L_2 meteorological data to 0.125° ($1/8^\circ$), and set the resolution of L_1 to 0.03125° ($1/32^\circ$), these are summarized in Table 1. We then run the model from 1965 to ~~2023~~ 2020, including a warm-up period of 5 years at the beginning.

Long-term in situ soil moisture data to validate the soil moisture output of mHM is not available within Belgium; so we expanded the model domain to cover parts of France, Germany and the Netherlands, where soil moisture observations are available from the International Soil Moisture Network (ISMN) (Dorigo et al., 2021). From the ISMN, we used data from the following networks: COSMOS (Zreda et al., 2008), GROW (Xaver et al., 2020), TERENO (Bogena et al., 2018), BFG-Nw and ORACLE, all shown in Figure 2.

2.2.2 mHM Soil Moisture simulation

mHM calculates water infiltration between soil layers using an exponential function that accounts for the nonlinearity of soil water retention (Samaniego et al., 2010; Livneh et al., 2015). Briefly, for a given soil layer, k , on pervious areas, the infiltration I_k into the layer is

Table 1: Summary of data sources

Dataset	Resolution (degrees)	Input format	Source
Meteorological data	1/8	NetCDF	E-OBS v30.0e
Leaf Area Index	1/512	NetCDF	GIMMS
DEM	1/512	ASCII Grid	SRTM
Geology	1/512	ASCII Grid	Global Lithological Map Database
Land Cover	1/512	ASCII Grid	Corine Landcover
Soil texture	1/512	ASCII Grid	Harmonized World Soil Database

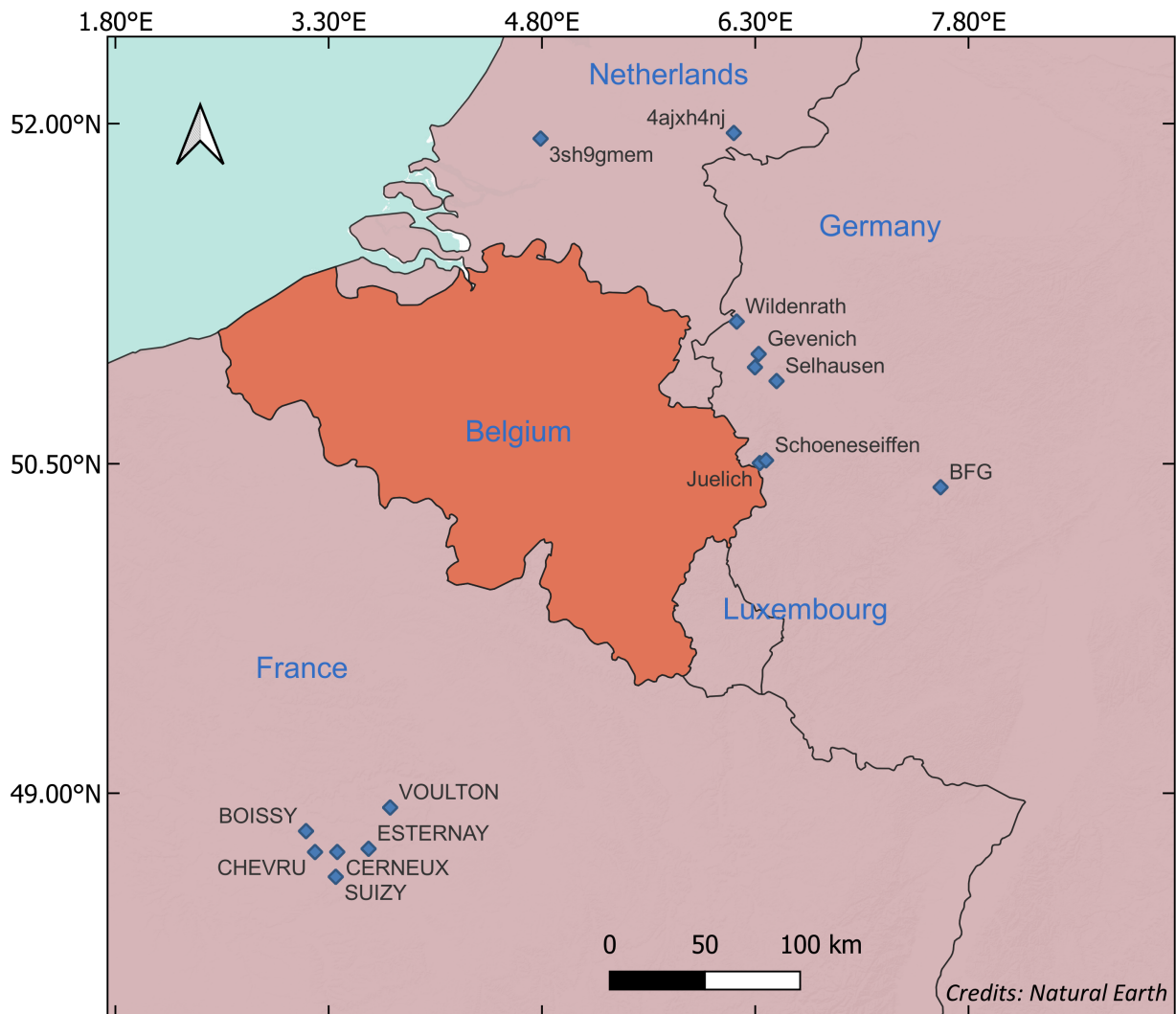


Figure 2: Locations of ISMN stations (blue diamonds) used to validate mHM soil moisture

determined by the equation:

$$I_k = I_{k-1} * \left(\frac{\theta_k}{\theta_{sat,k}} \right)^{\beta_k} \quad (1)$$

242 I_{k-1} represents the infiltration from the previous layer $k-1$, θ_k is the soil moisture
 243 of layer k , $\theta_{sat,k}$ is the saturation moisture content for the layer, and β_k is an exponential
 244 parameter that adjusts for the non-linear nature of soil moisture retention. Once infiltration
 245 is calculated, the model updates soil moisture θ_t by adding the difference between the layer
 246 infiltration I_t and actual evapotranspiration (ET_t) for the time step as;

$$\theta_t = \theta_{t-1} + I_t - ET_t \quad (2)$$

247 Actual evapotranspiration is calculated by reducing the potential evapotranspiration
 248 (PET) based on a soil moisture stress factor, f_{SM} , which varies depending on the soil mois-
 249 ture content.

$$ET = f_{roots} \cdot f_{SM} \cdot PET \quad (3)$$

250 f_{roots} is the fraction of roots in the soil horizon and f_{SM} is calculated using either the
 251 Feddes equation (Feddes, 1982):

$$f_{SM} = \frac{\theta - \theta_{pwp}}{\theta_{fc} - \theta_{pwp}} \quad (4)$$

252 or the Jarvis equation (after Jarvis, 1989):

$$f_{SM} = \frac{1}{\theta_{stress-index-C1}} \cdot \frac{\theta - \theta_{pwp}}{\theta_{sat} - \theta_{pwp}} \quad (5)$$

253 The model uses the MPR routine to compute the saturation moisture content, field ca-
 254 pacity (θ_{fc}) and wilting point (θ_{pwp}).

255 **2.2.3 Model evaluation**

256 The accuracy and spatial representativeness of absolute soil moisture values are strongly
 257 source-dependent (in situ or modelled), so direct comparisons between different datasets
 258 can be misleading (Koster et al., 2009; Ford and Quiring, 2019). On one hand, simulated
 259 soil moisture is highly dependent on the quality of meteorological forcings and the physical
 260 parameterisation of the model (Koster et al., 2009; Wang et al., 2011a; Nicolai-Shaw et
 261 al., 2015). On the other hand, in situ measurements are highly localized to the sensor
 262 location and are affected by the technology used by the sensor and the sufficiency of the
 263 calibration techniques (Peng et al., 2025). From a drought analysis perspective, the real
 264 information value of soil moisture is not in its absolute values but rather in its temporal
 265 variability metrics, such as anomalies and seasonal variability of soil wetness (Koster et
 266 al., 2009). This information value is generally more consistent and transferable between
 267 different sources when soil moisture is suitably normalised to have the same range and
 268 variability (Dirmeyer et al., 2004; Wang et al., 2011b). Koster et al., 2009 show that if

soil moisture from different sources differs only in their mean and standard deviation, then standardizing each time series (as in Equation 6) would generate nearly identical datasets of standard normal deviations (θ').

$$\theta' = \frac{\theta - \theta_m}{\sigma_m} \quad (6)$$

Where θ is the soil moisture at a given point and time of year, θ_m and σ_m are the mean and standard deviation of soil moisture, respectively, for the same point and time of year.

In our evaluation of the mHM soil moisture, we used this approach to analyze the level of temporal agreement between the standard normal deviations of mHM and in situ soil moisture from the corresponding depths at the selected ISMN stations (Figure 2).

For each in situ–modelled pair, we quantified the agreement in drought anomaly dynamics by calculating the Pearson correlation coefficient (r). To obtain an overall agreement across all sites, we first transformed the r values to the Fisher z -scale ($z = \text{arctanh}(r)$) to stabilize variance and avoid bias from the nonlinear r -scale. The z -values were then averaged to obtain \bar{z} , and finally back-transformed to yield $\bar{r} = \tanh \bar{z}$.

Prior to the comparison, we performed a quality check on the in situ data to flag and exclude potentially erroneous measurements. We considered only errors due to systematic drift in measurements over time (jumps or drops) and spiky measurements that are not explained by random noise. Here we used the quality control algorithms on in situ soil moisture developed by Dorigo et al., 2013 considering only stations that have at least 10 years of observations.

Because soil moisture is also coupled with runoff through the terrestrial water budget, we added an independent check for model simulations against daily river-discharge observations from the major river basins in Belgium. For this we used the inbuilt calibration feature of mHM and calibrated the model using data from river gauging stations all over the country, obtained from the Waterinfo database for Flanders (<https://waterinfo.vlaanderen.be/Meetreeksen>, last accessed March 2025) and the hydro-metric network of discharge in Wallonia (<https://hydrometrie.wallonie.be/home/observations/debit.html?>, last accessed May 2025). In total we used 91 gauging stations during the calibration period (2000–2023) and 155 stations to validate the model from 1970–1999.

2.3 Characterizing soil moisture droughts

To characterize soil moisture droughts, we use a monthly soil moisture index (SMI), following Samaniego et al., 2013, considering the total soil water content of the root zone up to a depth of 0.5 m (We limit our analysis to this depth since groundwater in some regions is shallower than 0.5m). For each month, grid cell soil moisture is expressed as a percentile relative to that month’s historical soil moisture and scaled to a range between 0 and 1.

The computation of SMI in this study is based on the methodology of Samaniego et al., 2010, which proceeds as follows. Firstly, the monthly soil moisture averaged over the ~~root~~

306 ~~zone-root-zone~~ depth (0.5 m for this study) is extracted and used to compute a probability
 307 distribution function (PDF) $f_t(x)$ for each grid cell as;

$$f_t(x) = \frac{1}{nh} \sum_{k=1}^n K\left(\frac{x-x_k}{h}\right) \quad (7)$$

308 Where, x is the soil moisture value at which the PDF is evaluated x_1, \dots, x_k represent
 309 the simulated monthly soil moisture values for ~~the~~ month t over the simulation period.
 310 Note that this conversion is done for each calendar ~~months-month~~ separately to account
 311 for inherent seasonality in SM simulations. K is a Gaussian kernel function and h is the
 312 bandwidth that controls the smoothness of the kernel (equation 8). The optimal value of h
 313 is computed using a cross-validation criterion.

$$K(x, x_k) = \frac{1}{\sqrt{2\pi}h^2} \exp\left(-\frac{(x-x_k)^2}{2h^2}\right) \quad (8)$$

314 The monthly grid cell SMI is then derived by integrating $f_t(x)$ and the resulting SMI
 315 values are classified into percentiles. Drought-affected grid cells are identified using a
 316 threshold percentile τ , which is commonly set at 0.2 (e.g., Svoboda et al., 2002; Samaniego
 317 et al., 2013; Samaniego et al., 2018). This means that for a given month, a grid cell is
 318 experiencing drought if the soil moisture value falls below the 20th percentile of values for
 319 that month. According to Svoboda et al., 2002, this percentile represents the threshold at
 320 which the magnitude of drought begins to damage crops, cause water shortages and present
 321 high risks of fire. Next, adjacent cells where $SMI \leq \tau$ (henceforth denoted as SMI_τ) at
 322 each timestep are consolidated to form drought clusters, which are defined by a minimum
 323 threshold area. Spatial clusters which share a minimum overlapping area at consecutive
 324 time steps are then joined to form multi-temporal clusters, each with a unique identity. For
 325 each cluster, the mean duration (months), areal extent from the onset to termination, and
 326 the total drought magnitude, which is the spatiotemporal integral of SMI_τ over the area
 327 affected, are computed. Following Samaniego et al., 2013, the magnitude of each event is
 328 computed as the space-time integral of the drought duration in months over the area under
 329 drought. This is represented mathematically as;

$$TDM = \sum_{t=t_0}^{t_1} \int_{A_t} [\tau - SMI_i(t)]_+ \quad (9)$$

330 t_0 and t_1 represent the onset and termination month of a multi-temporal drought event,
 331 A_t is the area under drought at timestep t expressed as a percent of the total domain area,
 332 and $[\cdot]_+$ means the magnitude is computed only for the positive part of the function. To
 333 avoid detecting small, isolated and short-lived dry spells as droughts, we specified a min-
 334 imum threshold area of 640 square kilometres (about 2% of total domain area) based on
 335 Samaniego et al., 2013 for an event to be considered as a drought, and an overlap area of
 336 the same size for two drought events at successive time steps to be considered as a single
 337 multi-temporal drought cluster.

3 Results

3.1 Model Performance Evaluation

3.1.1 Soil Moisture Simulations

The daily standardized anomalies of mHM-simulated soil moisture evaluated against in situ observations from the ISMN are shown in Figure 3. Of the 48 stations where in situ data was retrieved, 21 sites passed quality-control checks and were retained for validating the model outputs. The resulting comparison showed that the two datasets are highly temporally correlated, with a mean Pearson $\bar{r}=0.86$ (back-transformed averages from the Fisher z-scale), although the strength of the correlation varied with sensor depth and type. The correlation is lowest for the top 50 mm of the soil profile ($\bar{r}=0.81$ for all networks) and increases to 0.86 for the profile depths greater than 150 mm.

Even for the selected in situ sites, some still exhibited spurious spikes outside of random noise (shown by the red scatter points in Figure 3). We chose not to discard these points so as to preserve an adequate number of validation stations and to highlight the practical difficulty of obtaining perfectly reliable reference soil moisture data for validating model outputs.

Despite such outliers, the model simulations and ISMN observation showed similar temporal variability in soil wetness and dryness. The difference mainly occurred in the top 50 mm layer during very dry episodes when mHM produced more extreme negative anomalies than most sensors (Figure 3 (a-d)). This explains why the correlation between the datasets is the lowest at this depth. We attribute this divergence partly to a flooring effect of capacitive sensors, which tend to plateau at very low volumetric water contents, whereas the model continues to resolve further drying. For deeper layers, the intensity and duration of dryness were more consistent between both datasets. ~~Finally, we note that the strength of the agreement is also influenced by the~~

To evaluate how well the model simulates drought conditions, we investigated the drought-day detection skill (when the observed standardized anomaly fell below its 20th percentile) by counting hits (H ; days when both model and observations indicate drought), misses (M ; observed drought days not flagged by the model), false alarms (F ; days flagged as drought by the model but not by the observations), and correct negatives (C ; days when both indicate non-drought). (The methodology is described in more detail in Supplementary Text S1). From this analysis, we found that the model shows high skill in reproducing observed drought conditions, as it was able to detect 74% of observed drought days from the 21 stations. The false alarm rate was also only 5%, while the mean F_1 score (which summarizes the balance between misses and false alarms as $2H/(2H + F + M)$ was 75%. We attribute the differences in detecting droughts to the scale mismatch between mHM soil moisture, which represents average conditions over a grid cell, and the highly localized nature of point in situ measurements. Nevertheless, these metrics indicate that the model can be applied to study droughts.

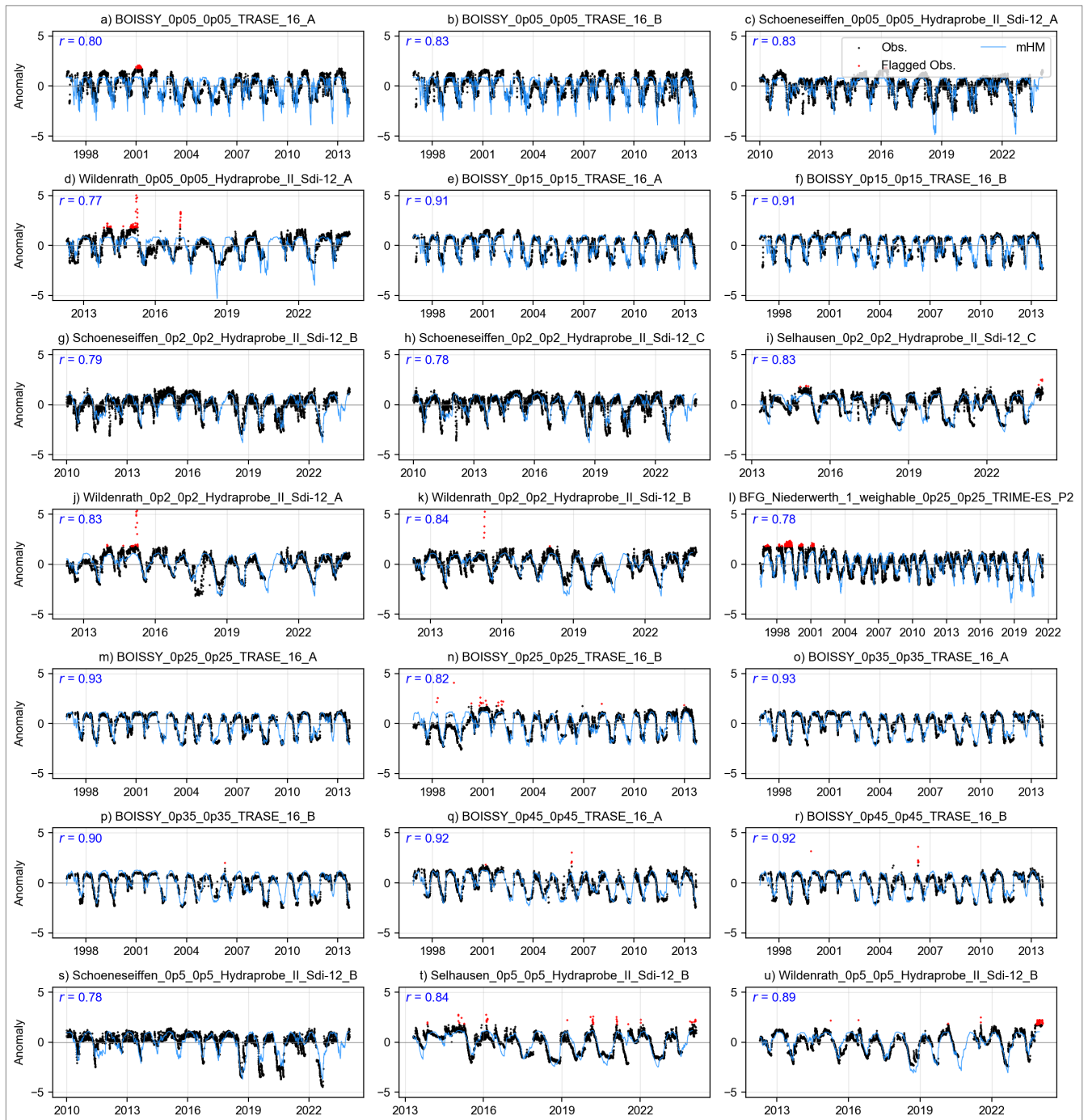


Figure 3: Comparison of standardized anomalies between mHM and in situ soil moisture at selected ISMN sites, ordered by increasing sensor depth. The red scatter points represent observed soil moisture values flagged as potentially erroneous. Titles follow the format station_topdepth_bottomdepth_sensortype, e.g., BOISSY_0p05_0p05_TRASE_16_A refers to the Boissy station with a sensor at 0.05 m depth and sensor type TRASE.

377

3.1.1 Streamflow Simulations

378

The skill of the model to represent daily simulated flow over the study domain is presented in Figure 4. For a robust evaluation of model performance, we retained only those stations

379

380 that had at least 10 years of data and excluded stations whose peak flow did not exceed
381 $10 \text{ m}^3 \text{ s}^{-1}$. The statistics show the model performed very well in simulating daily flows,
382 with a Regarding streamflow performance, the model shows good and spatially consistent
383 skill across the entire modelling domain and thus provides a reliable basis for analysing
384 soil moisture dynamics. We evaluated daily discharge at 168 gauging stations. During
385 calibration, the mean Nash-Sutcliffe Efficiency (NSE) of across stations was 0.62 and,
386 with 80% of stations having achieving NSE ≥ 0.5 in calibration. Validation statistics are
387 eomparable (a commonly used benchmark for satisfactory streamflow simulation). Model
388 performance during the validation period was also comparatively good, with a mean NSE
389 of 0.63 and 83% of stations exceeding an NSE of 0.50, which indicates good temporal
390 transferability. Spatially, as Figure 4 shows, the model shows consistent performance
391 across the domain. The model achieved the highest performance (NSE recording NSE
392 ≥ 0.75) in large basins, as the model could delineate the drainage extents of such basins
393 with higher accuracy. This delineation becomes more challenging in smaller basins and
394 especially where the topography is less pronounced, as is 0.5. The full details of the
395 streamflow evaluation, including the NSE definition, are provided in Supplementary Text S2
396 (Figure S1).

397 3.2 Decadal evolution of soil-moisture droughts

398 To summarize how soil-moisture drought behaviour evolves across decades, we use three
399 complementary metrics. First, we quantify the magnitude of each event using the Total
400 Drought Magnitude (TDM), which integrates drought severity over space and time and thus
401 allows drought events to be ranked consistently (Section 3.2.1). Second, in Section 3.2.1,
402 we describe how drought severity is distributed by quantifying the fraction of drought-affected
403 area falling into different severity classes (moderate, severe, extreme, and exceptional)
404 within each decade. These classes capture shifts in the composition of drought conditions
405 beyond just the total magnitude. Third, in Section 3.2.1, we quantify cumulative drought
406 exposure as the case in the northern part of the domain. Accordingly, the lowest model
407 performance was observed in gauging stations draining the smallest basins. In some cases,
408 anthropogenic modification of rivers such as canalization, diversions and diking, which is
409 common in the northern lowlands and which are not implemented in the model, explained
410 poor model performance at some gauging stations. Notwithstanding these few cases, the
411 results demonstrate that the model provides a reliable, spatially consistent basis for assessing
412 soil moisture dynamics over the country. total number of months in which each grid cell
413 experiences drought per decade (months need not be consecutive). This metric summarizes
414 how frequently drought conditions recur at a given location over a decade. For decadal
415 summaries, we defined decades starting from 1971 (i.e., 1971–1980, 1981–1990, ...) since
416 SPEI construction requires accumulated water-balance anomalies over preceding months
417 (January 1970 will thus not have SPEI-1 values, while January–March 1970 lacks SPEI-3
418 values. The first year with complete SPEI values is 1971).

419 Model performance at gauging stations across Belgium during calibration and validation

420 periods. The colour intensity and size of each circle are proportional to the NSE value. The
421 inset histograms show the distribution of NSE values across all stations for each period.

422 3.3 Multidecadal evolution of soil-moisture droughts

423 Figure 5 shows

424 3.2.1 Magnitude-based ranking of soil-moisture drought events

425 Figure 4 shows the magnitude of simulated soil moisture droughts over in Belgium between
426 1970 and 2023. The events are ranked by 2020 based on the Total Drought Magnitude
427 (TDM), the cumulative deficit in soil moisture below the chosen drought threshold ($SMI \leq$
428 $0.20 < 0.20$), integrated over the area and duration of the drought event. The biggest ten
429 events affected area and the event duration. To ensure an unambiguous severity ranking, the
430 events are ranked by TDM are colored and annotated with their corresponding periods and
431 when two events have similar TDM (difference $< 1\%$), ranks are resolved using a fixed
432 tie-breaker hierarchy: (i) average drought area (fraction of the domain with $SMI < 0.20$
433 averaged over the entire event), (ii) duration, and (iii) exceptional-class exposure (fraction
434 of $SMI < 0.020$ summed over the duration of the event). On the basis of this ranking,
435 Table 2 displays the corresponding metrics for the ten largest droughts during the period of
436 analysis. From an interdecadal perspective, the figure Figure 4 reveals three distinct drought
437 regimes. Three Beginning with the 1970s, three major drought events are apparent in the
438 1970s, which are dominated by the historic 1975–1977 droughts drought. Although this
439 event is commonly referred to as the 1976 drought, probably because that is when it peaked,
440 the analysis shows that its development in Belgium began back in the autumn of 1975 and
441 lasted for a record 16 months until the winter of 1977. By the end of the event, almost 63%
442 of the domain had experienced drought conditions, although this fluctuated at different
443 times over time¹. This event established a benchmark against which subsequent drought
444 events in droughts in many parts of Europe are commonly judged against compared. Our
445 analysis reflects this, as this event almost matches the most intense drought in Belgium
446 in the 53 years since 1970. Henceforth, this decade will be referred to as the 1971–1980
447 decade (we disregard 1970 because it is a calibration period for the drought analysis) during
448 the period of our analysis.

449 A relatively wetter hydroclimatic regime characterizes the three subsequent decades
450 (1981–1990, 1991–2000, and 2001–2010). This is observable in Figure 5 as indicated by are characterized by a comparatively wetter
451 hydroclimatic regime, reflected in the lower-magnitude drought occurrences. In these three
452 decades, only three drought events are big enough to feature events in Figure 4. Only three
453 events from this period appear in the top ten droughts, and even these ranked relatively low
454 in the TDM scale. The 1995–96 drought, the biggest of the three, however did persist for
455

¹The 63% figure is the mean fraction of the domain affected across all time steps during the drought; at individual times coverage ranged below and above this value, with a maximum of complete (100%) coverage when the drought peaked

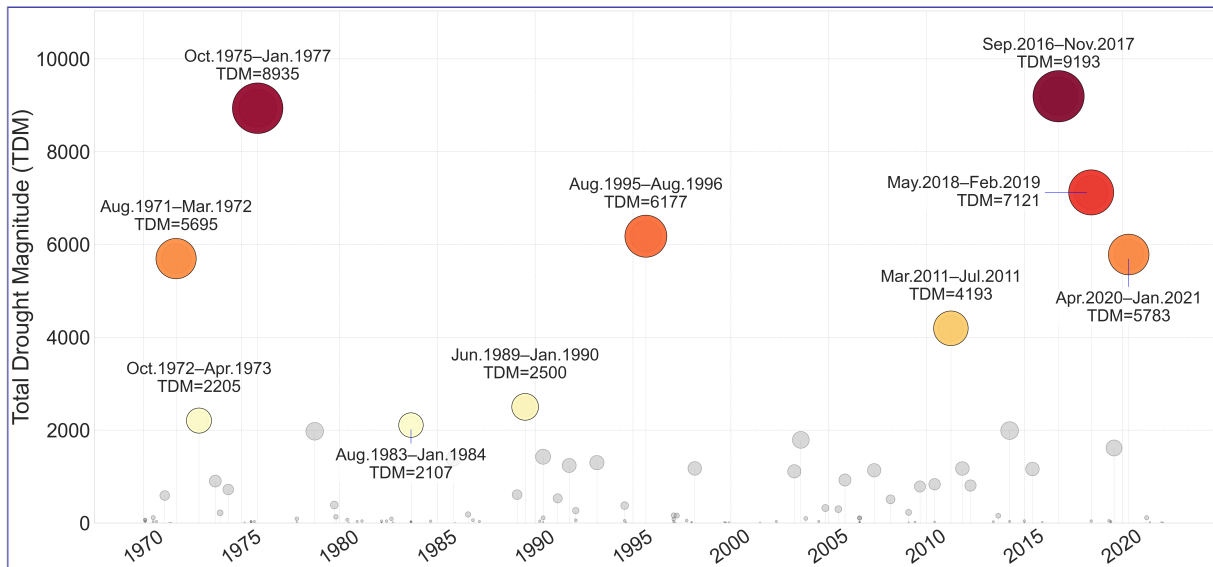


Figure 4: Duration and magnitude of drought events from 1970 to ~~2023~~, ~~2020~~. Each circle represents a drought event, positioned according to its start date (x-axis). The circle size is proportional to the Total Drought Magnitude (TDM) of each event. The ten most severe droughts, ranked by TDM, are highlighted with coloured markers, with their corresponding periods annotated. Events are ranked primarily by TDM; when two events have similar TDM (difference $\leq 1\%$), ranks are determined by peak affected area, then duration, then exceptional-class exposure (defined as $SMI < 0.02$).

456 ~~at least a year, and all rank relatively low by TDM. The largest of these, the 1995–1996~~
 457 ~~drought, nonetheless persisted for 13 months.~~
 458 A significant shift in drought frequency and severity emerged after 2011. Of the ten ~~highest~~
 459 ~~ranking biggest~~ droughts from 1971, ~~40%~~ ~~four~~ of them were recorded ~~in the 2011–2020~~
 460 ~~decade with three severe drought events clustered between 2011 and 2020, three of which~~
 461 ~~occurred~~ in rapid succession between 2016 and 2020. The 2016–2017 drought is the biggest
 462 in this ~~decade, matching period, exceeding even~~ the 1975–1977 drought by ~~magnitude,~~
 463 ~~TDM and~~ affected area (64%) and lasting nearly as long (15 months) ~~before it fully dissipated.~~
 464 ~~The 2018–19 droughts also rank highly although it lasted about 10 months but affected a~~
 465 ~~bigger area on average (, as shown in Table 2. The 2018–2019 drought also ranks among~~
 466 ~~the the largest events, exceeded in TDM only by the 2016–2017 and 1975–1977 droughts~~
 467 ~~(Table 2). Although it persisted for only 10 months, it affected a large fraction of the domain~~
 468 ~~on average (73%). This pattern has continued robustly into the 2020s, as underscored by the~~
 469 ~~2020–21 and 2022–2023 droughts . By cumulative magnitude, the 2022–2023 event, not~~
 470 ~~shown here, (lasted for 12 months between March 2022 and February 2023 with a TDM of~~
 471 ~~7870) ranks just below the 1975–1977 and 2016–2017 droughts. We have excluded drought~~
 472 ~~events %). Although some big droughts have occurred~~ after 2020 ~~from the subsequent~~
 473 ~~decadal, we have excluded these from our inter-decadal~~ analysis because the current decade
 474 is still incomplete. ~~In the subsequent analysis, the 2020–2021 is also only considered until~~
 475 ~~the end of 2020.~~

3.3 Area characteristics and shifts in drought-class composition

3.2.1 Decadal shifts in drought severity

While TDM provides a suitable event-ranking metric, it aggregates drought conditions over space and time and therefore does not directly indicate whether severity arises from widespread moderate drought or short periods of extreme conditions. To resolve this, we classified all the drought events into four severity classes following Svoboda et al., 2002: moderate drought ($0.1 \leq \text{SMI} < 0.2$), severe drought ($0.05 \leq \text{SMI} < 0.1$), extreme drought ($0.02 < \text{SMI} \leq 0.05$), and exceptional drought ($\text{SMI} \leq 0.02$). We then examined how the severity of droughts has evolved within and across decades, as shown in Figure 5. For conciseness we will examine the changes at both ends of the drought spectrum.

During the 1971–80 decade, droughts severity spectrum.

As Figure 5 shows, droughts during 1971–1980 were predominantly moderate ($0.1 \leq \text{SMI} < 0.2$). When they did occur, exceptional droughts did not affect more than exceptional droughts occurred, they remained spatially limited, peaking at below 30% of the domain at their peaks in during the 1971–1972 and 1976–1977. The figure also shows that 1975–1977 events (shown by the black dots in Figure 5). As the figure shows, these two droughts were disrupted by wetter spells which allowed re-establishment of normal to wet soil moisture conditions between drought phases. When accumulated over the decade, moderate droughts accounted for about 75% almost 80% of all grid-cell months affected by drought, while exceptional droughts, which are very rare by design, accounted for about 3% of drought-affected area, most of this occurring during 1975–1977 drought event (donut plots in Figure 5).

Normal-to-wet Between 1981 and 2010, the drought regime is characterized by predominantly normal-to-wet conditions interspersed with episodic, short-lived droughts dominate the spatiotemporal profile between 1981 and 2010. Decadal accumulations show. Decadal aggregates indicate that at least 80% of all drought occurrences during this time drought-affected grid-cell months during this period were moderate in intensity, while exceptional droughts constituted, on average, whereas exceptional drought contributed on average less than 1% of occurrences over the three decades (Figure 6). However, individual events (e.g., the 1995–1996 drought) still exhibited brief peaks of exceptional drought extent when exceptional conditions reached ~30% of the domain (Figure 5).

In contrast, the 2011–2020 decade period experienced more frequent and severe droughts, particularly towards the end of the decade (Figure 5). In comparison to the previous decades, the spatial footprint of exceptional droughts noticeably increased. At the peak of the 2011 and 2016–2017 droughts, more than droughts, exceptional droughts affected close to 70% of the domain, while during the 2016–2017 drought, about 40% of the drought-affected area was under exceptional drought, which did not previously occur even during the 1975–1977 event. This increase is reflected in the decadal drought area severity, where exceptional droughts accounted for 5.9% of drought-affected area, exceeding a

516 proportion that exceeds all the previous four decades combined –
517 (Figure 5).

518 **3.3 Decadal drought exposure**

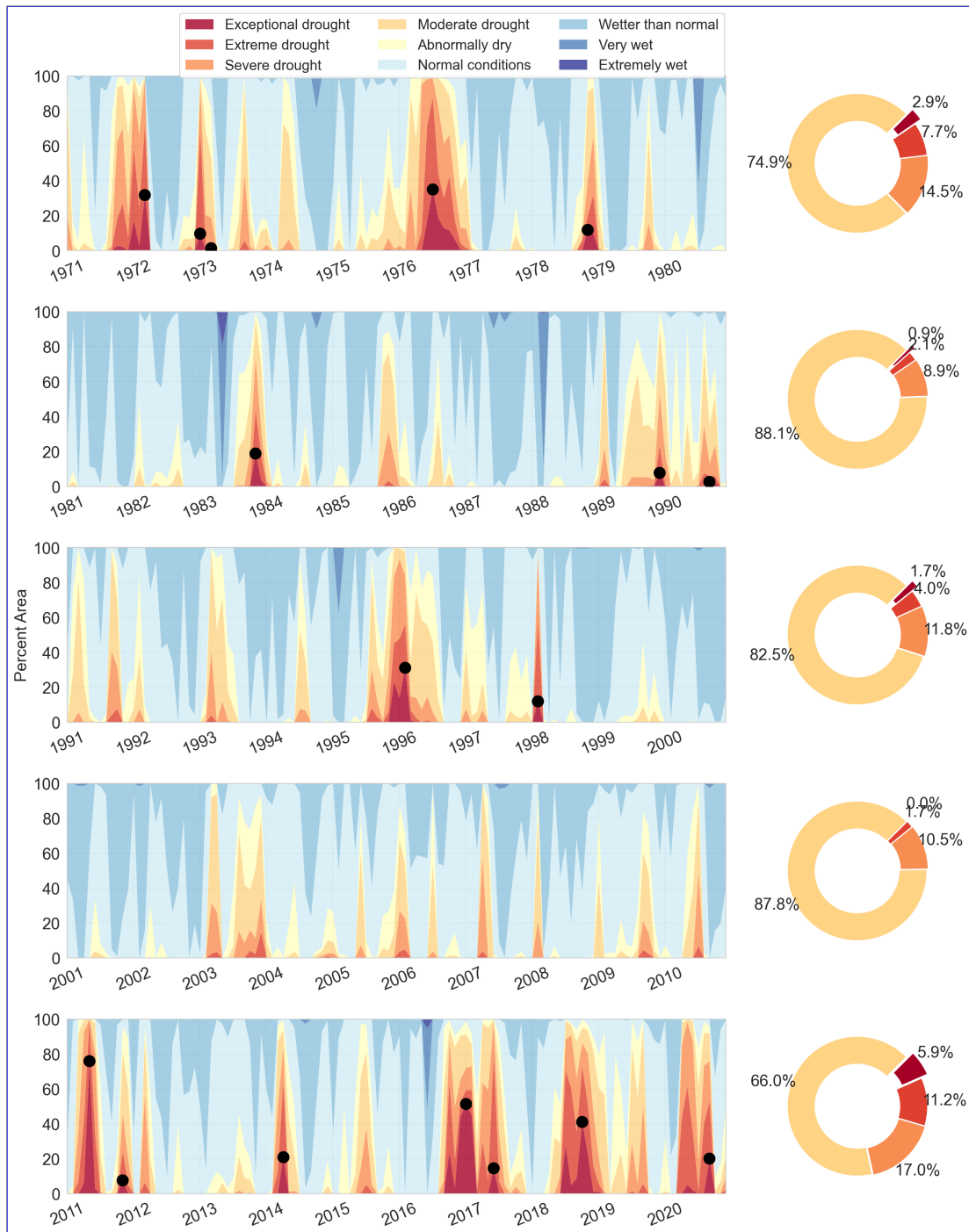


Figure 5: Decadal spatio-temporal evolution of soil moisture drought severity in Belgium, 1971–2020. For each decade (The stacked panels , (left) the coloured bands show the monthly percentage of land area falling into in each soil-moisture classes, from “class. Black dots mark the peak extent of exceptional drought ” to “extremely wet” ($SMI \leq 0.02$). The accompanying donut charts (right) aggregate only the months in which some part of the country was in summarize, for drought months only ($SMI \leq 0.20 \leq 0.20$); they display, the mean share of the drought-affected area that fell into in each drought class over the decade. Months ; months without drought contribute no area to the donut.

Figure 6 combines the temporal and areal characteristics of drought to illustrate the proportion of the domain experiencing varying degrees of soil-moisture drought severity through time. The categorization of drought into severity classes is based on Svoboda et al., 2002. The categories are clustered as follows:-

Table 2: The ten biggest soil moisture drought events in Belgium ranked by Total Drought Magnitude.

<u>Rank</u>	<u>Event period</u>	<u>TDM</u>	<u>Average affected area (%)</u>	<u>Duration (months)</u>	<u>Exceptional class exposure (%·mo)</u>
<u>1</u>	<u>Sep 2016–Nov 2017</u>	<u>9193.14</u>	<u>64.0</u>	<u>15</u>	<u>182.9</u>
<u>2</u>	<u>Oct 1975–Jan 1977</u>	<u>8934.97</u>	<u>62.6</u>	<u>16</u>	<u>103.4</u>
<u>3</u>	<u>May 2018–Feb 2019</u>	<u>7120.88</u>	<u>73.1</u>	<u>10</u>	<u>108.3</u>
<u>4</u>	<u>Aug 1995–Aug 1996</u>	<u>6177.27</u>	<u>60.3</u>	<u>13</u>	<u>69.8</u>
<u>5</u>	<u>Apr 2020–Jan 2021</u>	<u>5782.83</u>	<u>58.0</u>	<u>10</u>	<u>27.7</u>
<u>6</u>	<u>Aug 1971–Mar 1972</u>	<u>5694.68</u>	<u>72.9</u>	<u>8</u>	<u>57.3</u>
<u>7</u>	<u>Mar 2011–Jul 2011</u>	<u>4192.92</u>	<u>81.6</u>	<u>5</u>	<u>84.9</u>
<u>8</u>	<u>Jun 1989–Jan 1990</u>	<u>2500.37</u>	<u>51.5</u>	<u>8</u>	<u>8.0</u>
<u>9</u>	<u>Oct 1972–Apr 1973</u>	<u>2204.63</u>	<u>35.4</u>	<u>7</u>	<u>11.2</u>
<u>10</u>	<u>Aug 1983–Jan 1984</u>	<u>2107.37</u>	<u>47.0</u>	<u>6</u>	<u>22.4</u>

3.2.1 Decadal drought exposure

Complementing the temporal and spatial analyses, Figure 7 illustrates decadal drought persistence, Figure 6 illustrates decadal cumulative drought exposure, expressed as the total number of months in which each grid cell experienced $\text{SMI} \leq 0.2$ in a decade. The results agree with those of the previous analysis. During 1971–1980, the domain accumulated between 12 and 36 drought months, with a domain-wide mean of about 24 months per grid cell (2.4 months/year) (Figure 6 inset histogram).

Domain-wide improvements in moisture conditions are apparent in the next three decades. The mean cumulative totals fell to 13 months in 1981–1990 (1.3 months/yr), 17 months in 1991–2000 (1.7 months/yr.), and 14 months in 2001–2010 (1.4 months/yr).

As with the other metrics, drought persistence peaked in 2011–2020, cumulative drought exposure peaked in 2011–2020. The domain accumulated between 24 and 48 months of drought over the decade, and the domain-wide mean rose to 37 months, or 3.7 months per year (Figure 7). To put this into perspective, this amounts to roughly three continuous years of soil-moisture drought within the decade. This cumulative exposure is more than twice that of each of the three preceding decades (1981–1990, 1991–2000, 2001–2010) and about 1.5 times higher than the previous driest decade, 1971–1980.

To test whether 2011–2020 was statistically drier than the preceding four decades, we applied a non-parametric bootstrap to the per-pixel cumulative drought durations ($\text{SMI} \leq 0.20$) and to the subset of exceptional drought months ($\text{SMI} \leq 0.02$). For each decade, we generated 100,000 bootstrap samples by resampling grid-cell drought durations with replacement, calculated the mean for each sample, and used the 2.5th and 97.5th percentiles of the resulting distribution to derive the 95% confidence interval (CI) of the sample mean.

The statistical analysis concludes that 2011–2020 was indeed the driest decade of the five decades, both in terms of total drought duration and exposure to exceptional droughts. Over the decade, Belgium accumulated a mean drought period of 37 months (CI: 36.9–37.2 months), significantly higher than in 1971–1980 (mean=25.65 months [CI: 25.6–25.8]), which is the next driest decade (Figure 8-7(a)). The lower bound of the 2011–2020 decade CI lies 11 months above the upper bound of the 1971–1980 period and far higher than those experienced in the three decades in between (1981–1990: mean 13 months [CI: 12.92–13.15], 1991–2000: mean 16.9 months [CI: 16.80–16.95] and 2001–2010: mean 13.52 months [CI: 13.46–13.59]).

A similar contrast emerges for the most severe drought (Figure 8-7(b)). The 2011–2020 decade accumulated 4.3 months of exceptional drought on average (CI: 4.28–4.38), more than the combined total of the four earlier decades. None of the previous decades reached a mean of 2 months of exceptional droughts. 1971–1980 accumulated 1.94 months (CI: 1.89–1.98), 1981–1990 only 0.35 months (CI: 0.34–0.36), 1991–2000 0.80 months (CI: 0.79–0.84), and 2001–2010 experienced virtually no exceptional drought. In cumulative terms, more than half of all exceptional drought months in the five-decade record occurred between 2011 and 2020.

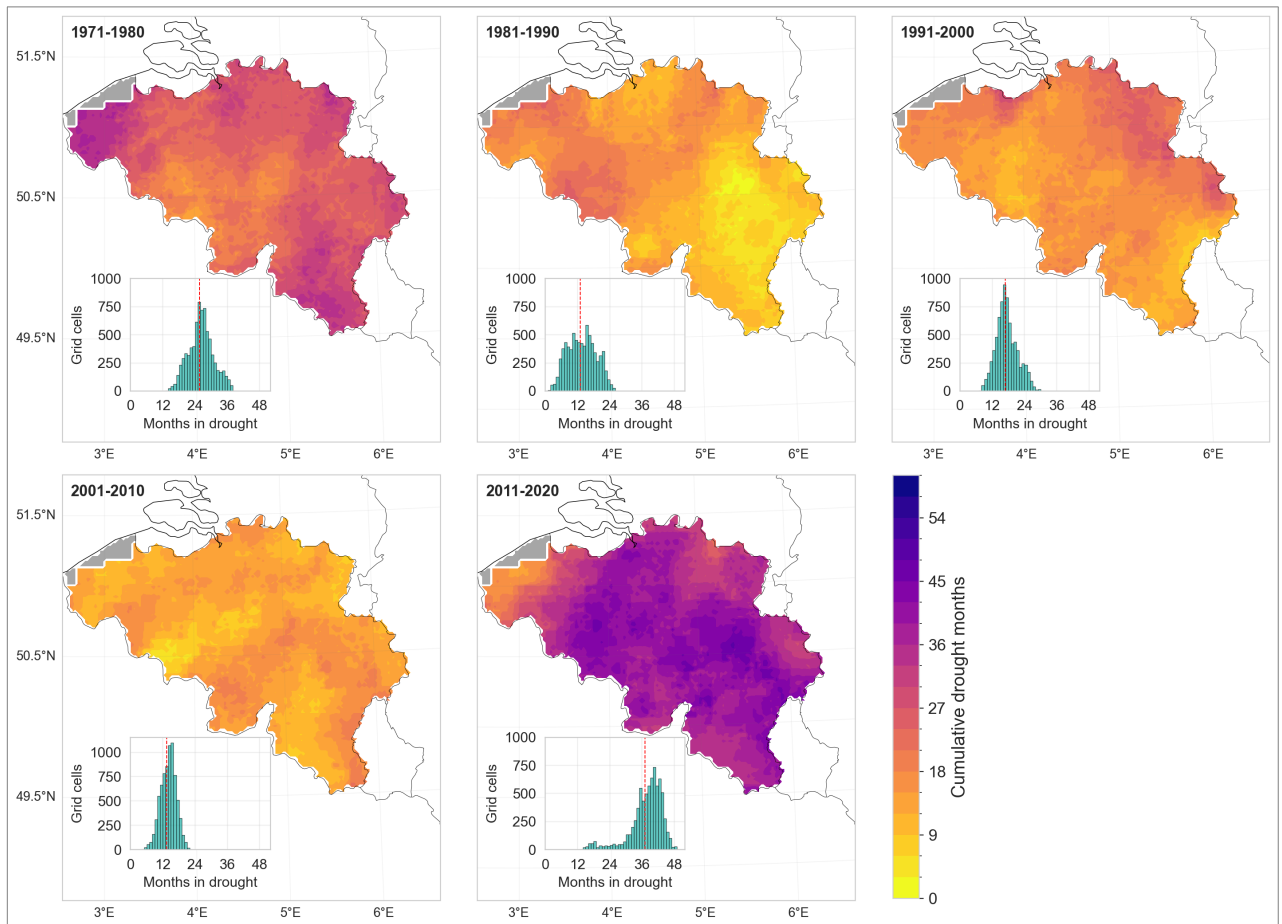


Figure 6: Distribution of Cumulative decadal drought exposure expressed as the number of months within each decade that a grid cell experienced drought conditions ($SMI \leq 0.2$). The inset histograms show the frequency distribution of cumulative time under drought for all grid cells. The red dashed line indicates the mean duration. EObs data is missing for the region shaded grey.

3.3 Divergence Between Soil Moisture between soil moisture and Precipitation-Based Drought Indicators To investigate SPEI droughts

To examine how precipitation-based drought indicators reflect land-surface-land-surface moisture stress, we compared ~~the~~ SMI and SPEI during the patterns during the three most severe soil moisture drought events ranked by TDM (total drought months (TDM): 1975–1977, 2016–2017, and 2018–2019). ~~Since the~~. Because SMI is computed on a monthly timescale, we ~~calculated the accumulated difference between EObs precipitation and potential evapotranspiration~~ derived the climatic water balance (precipitation minus potential evapotranspiration) from E-OBS and calculated SPEI at one- and three-month timescales and used the SPEI accumulation periods. Pixel-wise SPEI-1 and SPEI-3 were computed using the SPEI package developed by Vonk, 2024 to compute pixel-wise 1-month SPEI (SPEI-1) and three-month SPEI (SPEI-3). We also limit. We limited the accumulation period to 3 months as this is what is three months because this timescale is currently used in operational drought mon-

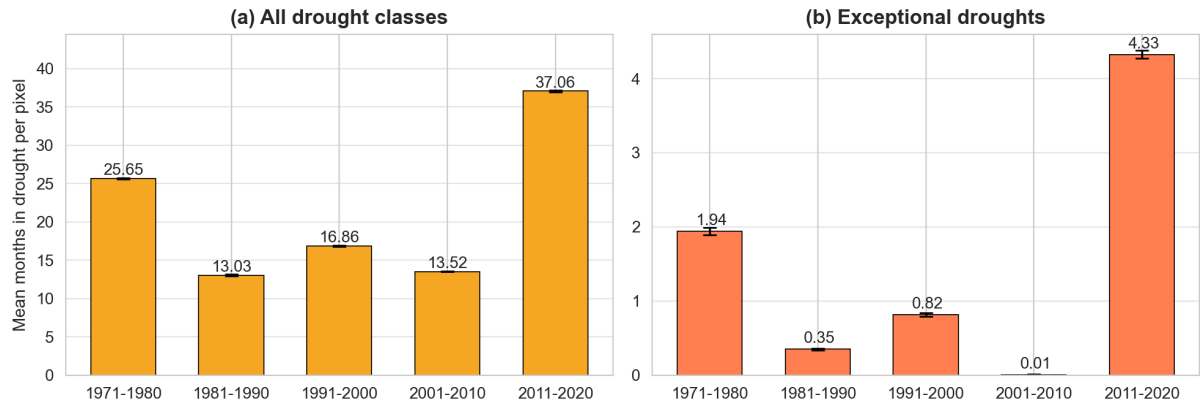


Figure 7: Decadal pixel-wise cumulative drought persistence exposure. The bars show the mean number of months each grid cell spent in drought per decade (not necessarily consecutive), with 95% bootstrap confidence intervals (black whiskers) for (a) All drought classes ($\text{SMI} \leq 0.20$) and, (b) Exceptional exceptional drought only ($\text{SMI} \leq 0.02$).

572 itoring in ~~the country. As SPEI is an~~ Belgium. Since SPEI is anomaly-based rather than
 573 a percentile-based index, we associated an SPEI value of -1.0 to an SMI value of 0.2 . $\text{SPEI} = -1.0$ with $\text{SMI} = 0.2$ to represent the threshold for moderate drought severity, according
 574 to the guidelines by Svoboda et al., 2002. at least moderate drought, following the drought
 575 severity guidelines of Svoboda et al., 2002. We evaluated the differences between indices in
 576 terms of (i) anomaly magnitude, (ii) drought persistence (maximum number of consecutive
 577 months under at least moderate drought within an event), and (iii) cumulative drought
 578 exposure (total number of months, not necessarily consecutive, under at least moderate
 579 drought within the event window).

581 Across the three drought events, SMI generally exhibits more persistent negative anomalies
 582 In terms of anomaly magnitude, SMI generally indicated stronger and longer-lasting deficits
 583 than SPEI-1 and, to a lesser extent, SPEI-3 (Figure ??8). SPEI-1 is highly responsive
 584 responds strongly to short-lived rainfall deficits and surpluses precipitation anomalies that
 585 may not immediately alter translate into changes in root-zone storage; this sensitivity captures
 586 meteorological conditions which differ from soil moisture conditions that integrate past
 587 deficits through slow infiltration and plant uptake. As expected. By design, SPEI-3 smooths
 588 some of the short-term variability inherent to in SPEI-1 and more closely mirrors the
 589 temporal pattern resembles the temporal evolution of soil-moisture anomalies. Even so,
 590 for our domain, SPEI-3, but still tends to underestimate the persistence and the magnitude
 591 of deficits deficit magnitude relative to SMI. For example, of the three drought over our
 592 domain (Figure 8). Among the three events, SMI shows that soil moisture anomalies were
 593 strongest during the indicated the strongest soil moisture deficits during 2016–2017 drought
 594 (SMI near zero). (with SMI approaching zero), which is not reflected in either SPEI-1 or
 595 SPEI-3 on the other hand, appears to underestimate the extent of this difference between
 596 the three droughts. SMI also shows a stronger persistence in time, which implies that
 597 soil moisture has a higher inertia and responds not only to the magnitude but also to the

598 ~~sequence of meteorological anomalies.~~

599 ~~When analyzing drought recovery, the same pattern also emerges.~~ Although the
600 2016–2017 drought was interrupted by intermediate wet conditions during March and
601 April 2017, leading to partial recovery, this wet spell did not split the event because the
602 month-to-month overlap in drought area remained above the 640 km² merging threshold,
603 and the drought therefore remained a single multi-temporal event.

604 We also found that SMI-based droughts exhibited higher persistence than SPEI-based
605 droughts. Median persistence for SMI was 9 months in 1975–1977, 6 months in 2016–2017,
606 and 7 months in 2018–2019 (Table 3). In comparison, SPEI-1 ~~reacts fastest and shows an~~
607 ~~earlier termination of droughts~~. Although the exact pattern of recovery is event-specific,
608 drought recovery follows the same general order: short-term water balance anomalies (SPEI-1) ~~normalize~~
609 ~~first followed by seasonal water balance anomalies~~ (shows much shorter median persistence
610 (3 months in 1975–1977 and 2 months in both 2016–2017 and 2018–2019), while SPEI-3)
611 before soil moisture conditions emerge out of drought. This pattern is most evident during
612 the drought events of 1975–1977 is closer to SMI but remains lower (7 months in 1975–1977
613 and 2018–2019 (Figure ??). During the 5 months in both 2016–2017 and 2018–2019).

614 The same pattern is evident for cumulative drought exposure. Median cumulative
615 exposure for SMI was 10 months in 1975–1977 ~~drought event, all the indices show that~~
616 ~~the drought-affected area peaked by August 1976. According to the evolution of SPEI-1 and~~
617 ~~2016–2017 and 8 months in 2018–2019, compared with 4, the drought had virtually terminated~~
618 ~~by around November 1976. Yet, by this time almost half of the domain area was still~~
619 ~~under 6, and 3 months for SPEI-1 and 7, 8, and 6 months for SPEI-3 drought while SMI~~
620 ~~shows closer to 90% of the domain was still under drought. By the time SPEI-3 drought~~
621 ~~terminates in January 1977, more than one-third of the domain was still under SMI drought,~~
622 ~~which took until February 1977 to terminate. A similar sequence of recovery is observed~~
623 ~~during the 2018–2019 drought. The 2016–2017 drought was interrupted by intermediate~~
624 ~~wet conditions during March and April 2017 which led to partial drought recovery and~~
625 ~~consequently a smaller margin between SPEI-3 and SMI recoveries.~~ (Table 3, additional
626 maps in Supplementary Text S3, Figures S3 and S4).

627 We stress that these differences ~~This systematically longer persistence and exposure~~
628 ~~shown by the SMI indicates that soil moisture droughts last longer than precipitation-based~~
629 ~~droughts because transient precipitation events do not necessarily translate into root-zone~~
630 ~~recovery. Additional description on the patterns of SMI and SPEI recovery is presented in~~
631 ~~Supplementary Text S3.~~

632 The differences presented herein do not imply that one indicator is necessarily *bet-*
633 *ter*; rather, they are all useful for demonstrating how a drought shock progressively propa-
634 gates through different components of the hydrological system. Precipitation-based indices
635 like SPEI reflect short-term meteorological inputs that may still be agriculturally meaning-
636 ful. As Figure ??-8 shows, rainfall events during dry ~~summers periods~~ may not replenish
637 deeper soil moisture due to immediate losses through evapotranspiration, yet these events
638 can still temporarily alleviate plant water stress, especially for fast-responding, shallow-

639
640
641
642
643

rooted crops or annual crops. The recovery of SPEI out of drought conditions may thus signal 'relief' that is real, albeit short-lived and limited in scope. On the other hand, SMI-based drought analysis better captures the persistence of land surface water deficits and the residual moisture stresses that continue to affect the dependent ecosystems (e.g., perennial deep-rooted vegetation) long after meteorological conditions have normalized.

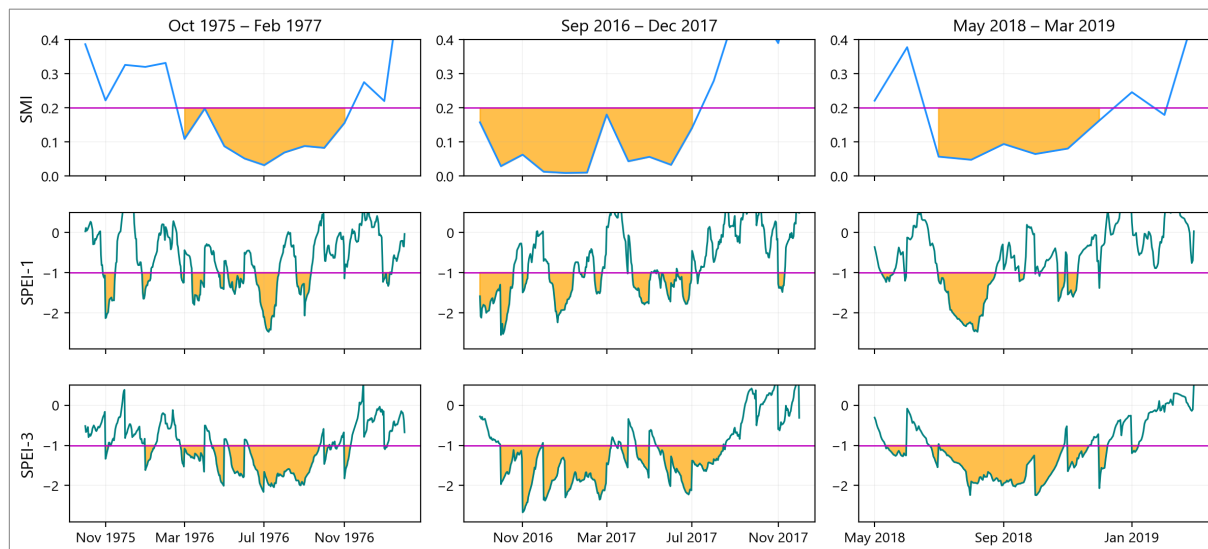


Figure 8: Comparison of domain-average SMI, SPEI-1, and SPEI-3 time series during the three biggest drought events up to 2020. The orange shaded areas indicate drought conditions, defined as $SMI \leq 0.2$ and $SPEI \leq -1.0$. The horizontal magenta lines mark the drought threshold for each index.

Table 3: Evolution of area affected by Quantified drought persistence and cumulative drought exposure during the three biggest drought major events (1975–1977, represented using the three indices. The thresholds for SPEI-2016–2017, and 2018–2019) for SMI are as described, SPEI-1, and SPEI-3. Values represent the median across all grid cells in Figure ?? the domain. For cumulative exposure, we additionally report the spatial maximum (in brackets), which represents the time until the last grid cells recover above the moderate-drought threshold within the event window.

Index	Max. consecutive months (persistence)			Total drought months (cumulative exposure)		
	1975–1977	2016–2017	2018–2019	1975–1977	2016–2017	2018–2019
SMI	9	6	7	10 (16)	10 (15)	8 (10)
SPEI-1	3	2	2	4 (7)	6 (8)	3 (5)
SPEI-3	7	5	5	7 (13)	8 (12)	6 (9)

644
645
646
647

4 Discussion

This extended temporal analysis of soil moisture droughts over Belgium offers new insights on the severity of recent droughts in the country. Without such a long-term, multi-decadal viewpoint, the recent intensification of drought severity and frequency might be mistakenly

648 viewed as isolated, transient events rather than as indicators of a potential shift in the climate
649 regime. These changes, despite the absence of significant linear trends, also raise important
650 questions regarding potential non-linear transitions in regional hydro-climatic equilibria, to
651 which we find answers by studying longer reconstructions of the European drought patterns
652 from other studies.

653 Our findings ~~are consistent with~~ fit into the wider pan-European narrative of intensifying
654 droughts over the continent in the 21st century. García-Herrera et al., 2019 showed that
655 drought conditions covered 90% of central-western Europe from July 2016 to June 2017,
656 with 25% of the area in record-breaking severity. This drought led to widespread impacts
657 of agriculture, water supplies and hydropower production and was the most severe drought
658 Europe had faced between 1979 and 2017. Longer historical reconstructions of European
659 droughts by Hari et al., 2020 and Rakovec et al., 2022 show that the occurrence of the
660 consecutive European summer droughts of 2018–2019, where 50% of Central Europe was
661 under extreme drought conditions, is unprecedented in the last 250 years (since at least
662 1766). In their synthesis of the effect of this drought on crop yields, the same study found
663 that the drought reduced maize yields in western Europe by 20-40% and caused about a
664 10% loss in barley yields for a majority of European countries. By dating stable tree-ring
665 isotopes to reconstruct the summer hydroclimate of central Europe from 75 BCE to 2018
666 CE, Büntgen et al., 2021 found that the recent succession of extreme European summer
667 droughts between 2015 and 2018 are unprecedented in the previous 2,110 years.

668 ~~Studies~~ Various studies attribute atmospheric circulation patterns and the potential role
669 of anthropogenic warming as the dominant drivers of these drought dynamics. Ionita et
670 al., 2020 link the sustained period of spring droughts in Europe between 2007 and 2020
671 to a prevalence of anticyclonic and a persistent blocking high over the North Sea. These
672 conditions deflect westerly storms and increase temperature due to a lengthened sunshine
673 duration. This consequently increases evapotranspiration, which has been found to amplify
674 European summer droughts (Teuling et al., 2013). García-Herrera et al., 2019 observed that
675 high-latitude atmospheric blocking contributed to the drought conditions over northwestern
676 Europe in 2016–2017 by decreasing moisture transport from the Atlantic Ocean. Hari et al.,
677 2020 similarly attributed the intensification of the 2018-2019 drought to anticyclonic cir-
678 culation, which caused a blocking that increased temperature anomalies to +2.8 K in central
679 to northern Europe (Rakovec et al., 2022). These patterns are projected to persist in the
680 future as anthropogenic warming weakens the temperature gradient between the polar and
681 mid-latitude regions and ~~fluctuate~~ fluctuates the strength of the jet stream and the persis-
682 tence of extreme weather events (Cohen et al., 2014; Dai et al., 2019; Ionita et al., 2020).
683 Europe-wide studies show that anthropogenic warming will worsen droughts and events
684 ~~with~~ of the nature of severity as the 2018–2019 drought will become routine, persist longer
685 and affect a larger proportion of area (Samaniego et al., 2018; Hari et al., 2020; Rakovec
686 et al., 2022). These emphasize the need to continue strengthening drought monitoring and
687 investing in drought preparedness and mitigation measures.

688 On the comparison between precipitation and soil-based drought indicators, we stress

689 that these indicators are useful for different components of the hydrological system. SPEI-1
690 and SPEI-3 may suit analyzing drought patterns in shallow soil layers and shorter temporal
691 scales but are limited for indicating drought persistence deeper in the soil or in complex
692 ecosystems due to their ignorance of land-ecosystem interactions (Xu et al., 2021; Peng
693 et al., 2024). When assessing drought impacts on ecosystems, groundwater recharge, or
694 perennial vegetation like forests, the divergence between meteorological and soil mois-
695 ture signals can become complex. In such systems, soil properties such as hydrophobicity
696 during prolonged dry periods can lead to highly uneven infiltration (Gimbel et al., 2016;
697 Filipović et al., 2018). Heavy summer rainfall may not be absorbed uniformly across the
698 soil profile, but instead run off or infiltrate preferentially along cracks, roots, or macrop-
699 ores, sometimes bypassing the upper root zone. While this limits the ability of standard soil
700 moisture indices to reflect actual water availability near the surface, it may still benefit deep-
701 rooted vegetation like trees by replenishing deeper soil layers (Zhu et al., 2015; Duniway et
702 al., 2018). Assessing drought stress and recovery in these systems thus requires models and
703 indicators that account for vertical and spatial heterogeneity in infiltration and root water
704 uptake (e.g., Shen et al., 2025), rather than relying solely on averaged or surface-weighted
705 soil moisture metrics. Further, while it may be argued that SPEI at longer accumulation
706 periods (e.g., 6, 9 or 12 months) can lead to a closer resemblance of root-zone root-zone
707 moisture conditions, finding the appropriate accumulation lengths is dependent on land-
708 scape and soil characteristics (topography, rooting depth, soil hydrology and management
709 conditions) and climatic conditions, which can lead to a strong variation of drought charac-
710 teristics if the landscape is heterogeneous. Kumar et al., 2016 indeed found that applying
711 spatially variable accumulation periods achieves a higher correlation between precipitation-
712 based and groundwater drought indices, over a uniform domain-wide accumulation period,
713 even at long accumulation times.

714 Our findings are relevant beyond Belgium because the workflow used in this study
715 can be transferred to other regions provided that the meteorological forcing is available at
716 appropriate resolution, a hydrological or land-surface model is parameterized to represent
717 soil-water storage, and consistent long-term simulations can be produced. Extending the
718 analysis to other domains would allow the same drought dynamics addressed in this study to
719 be evaluated under different climate gradients, soil, land-cover conditions, and management
720 regimes.

721 From an operational perspective, the results support a monitoring strategy that complements
722 precipitation-based indices with soil-moisture-based indicators rather than interchanging
723 them. As we have shown, precipitation-based indices are useful for tracking meteorological
724 anomalies and can provide early signals of emerging drought risk, but they may not capture
725 persistent impacts when land-surface memory sustains root-zone deficits after rainfall resumes.
726 In an operational system, precipitation-based indices can be used for early warning, while
727 a root-zone soil moisture drought indicator is better utilized to track agricultural drought
728 development and recovery and to assess when conditions have returned to normal in the
729 soil profile. These outputs can be integrated into management decisions by linking drought

730 phase and persistence to sector-relevant decisions. For example, soil-moisture drought
731 persistence is directly relevant for agricultural advisories that inform planting and irrigation
732 planning and signaling crop yield risk and the risks associated with the occurrence of
733 wildfires or floods that can occur due to seasonally saturated soils. Slow recovery in soil and
734 catchment storage after meteorological drought can also inform water supply preparedness
735 and groundwater management, since water resources often show a delayed return to normal
736 conditions (Yang et al., 2017). For inland navigation and low-flow management, combining
737 soil moisture drought information with streamflow indicators can help distinguish short,
738 transient precipitation deficits from longer-lasting, storage-driven drought conditions. In
739 practice, monthly updates of a root-zone soil moisture drought map, paired with precipitation-based
740 indices, would support earlier identification of drought evolution and lead to more realistic
741 expectations for recovery following intermittent wet periods (Van Loon et al., 2024).

742 **5 Limitations and future work.**

743 Our results rely on the evaluation of model-derived soil moisture conditions, which are
744 inevitably constrained by structural, parametric, and forcing uncertainties that we did not
745 explicitly evaluate. Choices of the mapping between drought categories (e.g., SPEI = -1.0
746 vs. SMI \leq 0.2) and a uniform accumulation period over the whole domain (for SPEI analy-
747 sis) also introduce additional subjectivity. ~~mHM model does not also~~ The mHM model also
748 does not account for anthropogenic factors such as irrigation, groundwater abstraction, tile
749 drainage and artificial canals, and land management conditions, which affect the hydrology
750 of the domain. Future work can partially offset these limitations by quantifying uncertainty
751 using ensembles of forcings, investigating model parameters to derive confidence intervals
752 for drought magnitude, area, and timing, incorporating human water use and irrigation pro-
753 cesses, or assimilating independent observations (such as in situ or remotely sensed soil
754 moisture and terrestrial water storage) to better constrain states and evaluate the joint be-
755 haviour of multiple drought indicators alongside observed impacts.

756 **6 Conclusion**

757 ~~Our~~ This study provides a multi-decadal (1971–2020), high-resolution ~~analysis of rootzone~~
758 ~~soil moisture dynamics over Belgium reveals that soil moisture droughts experienced in the~~
759 ~~country during the 2011–2020 decade were the worst the country had experienced since~~
760 ~~at least 1971. Our analysis shows that droughts in 2011–2020 occurred nearly twice as~~
761 ~~frequent compared to the preceding three decades and exceeded even the historically severe~~
762 ~~droughts of the 1970s in both duration and intensity. By studying recent patterns in droughts~~
763 ~~over Europe, we found that this pattern is part of a broader, continent-scale shift toward~~
764 ~~more persistent droughts. Studies show that the recent rapid succession and increased~~
765 ~~severity of droughts in the latter part of the 2010s is unprecedented even in millennial~~
766 ~~timescales, an indicator that these anomalies might not be occurring within a stationary~~

767 climatic regime. These could rather be signals of a transition towards conditions where
768 droughts become longer and recur more frequently, driven by large-scale atmospheric blocking
769 events that favour the persistence of higher temperatures that enhance evapotranspiration.

770 This study also shows that characterizing agricultural droughts using indices based on
771 soil moisture offers a more holistic representation of land surface water stress compared
772 to precipitation-based drought indices. While current drought assessments in Belgium
773 rely upon meteorological indices (SPI and SPEI) reconstruction of root-zone soil moisture
774 droughts over Belgium. Using event-based severity metrics that quantify drought duration,
775 spatial extent, and intensity, this study shows that these indices can underestimate the
776 persistence and severity of soil moisture drought conditions in the root zone, which often
777 lag meteorological recovery, due to the memory effect of the land surface we show that
778 droughts in 2011–2020 occurred about 1.5 times as frequently as during the preceding
779 decades (1971–2010). The 2011–2020 decade also exhibits the highest share of exceptional
780 drought, exceeding the cumulative occurrence of exceptional drought across all earlier
781 decades in the record.

782 By comparing soil-moisture drought (SMI) with precipitation-based indicators (SPEI-1
783 and SPEI-3) for the three most severe events, we show that precipitation-based indices
784 systematically underestimate drought persistence and cumulative exposure relative to root-zone
785 soil moisture. In particular, soil moisture droughts persist longer and recover more slowly
786 than meteorological anomalies, reflecting land-surface memory. Including soil moisture
787 monitoring in drought observatories thus offers the added value of capturing lingering
788 stresses on agriculture and ~~ecosystem~~ecosystems, which can persist long after meteorological
789 conditions have normalized. This ~~gives~~ provides decision-makers a better with a
790 more complete view of drought severity and duration and guides them on how to devise
791 the appropriate supports targeted response and mitigation efforts. Lastly, as anthropogenic
792 warming worsens the occurrence of droughts, recognizing and proactively planning for
793 this evolving drought paradigm will be crucial for ensuring the resilience of water resource
794 management, agriculture, and ecosystems in a warming climate

795 The reconstructed drought record and event-based metrics presented in this study provide
796 a consistent basis for benchmarking recent droughts against historical variability and for
797 supporting drought monitoring and management.

798 **Author Contributions:**

799 KL, RK and OR formulated the study and set up the model simulations. KL analyzed
800 the data and prepared the figures with contributions from OR, RK and SD. All authors
801 contributed to writing and reviewing the contents of the manuscript. All authors read and
802 approved the contents of the final manuscript.

803 **Acknowledgements:**

804 We acknowledge the work of Jens Wilhelmi (BFG_Nw network) for providing data
805 in support of the International Soil Moisture Network. We also acknowledge the work of
806 Arnaud Blanchouin and ORACLE team of the Institut national de recherche en sciences
807 et technologies pour l'environnement et l'agriculture, France in support of the ISMN. We
808 are grateful to the High Performance Computing system of Vrije Universiteit Brussel for
809 providing the computational resources required to run the model and the analysis of model
810 outputs. We also acknowledge all the sources of data used in this study for providing the
811 data openly.

812 **Funding:**

813 The authors acknowledge the financial support of the Research Foundation – Flanders
814 (FWO) for funding the International Coordination Action (ICA) “Open Water Network:
815 Impacts of Global Change on Water Quality” (project code G0ADS24N). OR acknowl-
816 edges the Research Excellence in Environmental Sciences (REES) project of the Faculty of
817 Environmental Sciences, Czech University of Life Sciences Prague.

818 **Data Availability:**

819 All datasets used in this paper are openly available as described in the methodology text.

820 **Code Availability:**

821 The scripts used to arrive at the findings of this study ~~is~~ are available at:

822 https://github.com/klekarkar/pre_post_process_mHM.

823 The SMI analysis was carried out using the SMI package, available at:

824 <https://github.com/mhm-ufz/SMI>.

825 **Competing interests:**

826 At least one of the (co-)authors is a member of the editorial board of Hydrology and
827 Earth System Sciences.